


Spur Gear Tooth Pitting Propagation Assessment Using Model-based Analysis

Xi-Hui Liang¹ · Zhi-Liang Liu² · Jun Pan³ · Ming Jian Zuo¹ 

Received: 17 November 2016/Revised: 28 July 2017/Accepted: 11 October 2017/Published online: 8 November 2017
© The Author(s) 2017. This article is an open access publication

Abstract Tooth pitting is a common failure mode of a gearbox. Many researchers investigated dynamic properties of a gearbox with localized pitting damage on a single gear tooth. The dynamic properties of a gearbox with pitting distributed over multiple teeth have rarely been investigated. In this paper, gear tooth pitting propagation to neighboring teeth is modeled and investigated for a pair of spur gears. Tooth pitting propagation effect on time-varying mesh stiffness, gearbox dynamics and vibration characteristics is studied and then fault symptoms are revealed. In addition, the influence of gear mesh damping and environmental noise on gearbox vibration properties is investigated. In the end, 114 statistical features are tested to estimate tooth pitting growth. Statistical features that are insensitive to gear mesh damping and environmental noise are recommended.

Keywords Mesh stiffness · Mesh damping · Gear dynamics · Vibration · Statistical feature · Dynamic simulation

1 Introduction

Gearbox is one of the most widely used transmission systems in the world. However, due to high service load, harsh operating conditions or fatigue, faults may develop in gears [1]. Through observations at gearboxes used in Syncrude Canada Ltd, tooth pitting was a common failure mode [2]. When tooth pitting appears on gears, gear mesh stiffness reduces and correspondingly the vibration properties of gears change.

According to the American Society for Metals (ASM) handbook [3], gear pitting damage can be classified into five levels according to pitted areas as follows:

1. Some micro-pitting (pits with dimensions in the order of millimeters) and a few macro-pits on the pinion. No pitting on the gear.
2. Micro-pitting and appreciable macro-pitting on the pinion. Almost no pitting on the gear.
3. Micro-pitting and considerable macro-pitting on the pinion with one or more gross pits. Damage to both the pinion and the gear.
4. Macro-pitting over 50%–100% of the pinion tooth surface. Removal of metal thins the teeth and disrupts load sharing between teeth. Gear unit has greatly increased noise and vibration.
5. Macro-pitting all over the teeth with considerable gross pitting. Teeth are thinned so much by wear that the tips are becoming sharp like a knife.

Supported by Natural Science and Engineering Research Council of Canada (Grant No. RGPIN-2015-04897), International S&T Cooperation Program of China (Grant No. 2015DFA71400), National Key Research and Development Program of China (Grant No. 2016YFB1200401), and National Natural Science Foundation of China (Grant No. 51375078, 51505066).

✉ Ming Jian Zuo
ming.zuo@ualberta.ca

¹ Department of Mechanical Engineering, University of Alberta, Edmonton T6G 1H9, Canada

² School of Mechatronics Engineering, University of Electronic Science and Technology, Chengdu 611731, China

³ Key Laboratory of Reliability Technology for Mechanical and Electrical Product of Zhejiang Province, Zhejiang Sci-Tech University, Hangzhou 310018, China

Some researchers [4–7] created man-made tooth pitting on gears to experimentally explore fault symptoms of a gearbox. For example, in Ref. [8], three pitting levels were created using the electro discharge machining, namely, slight pitting, moderate pitting and severe pitting as shown in Figure 1. In these methods, vibration sensors are generally installed on the casing of bearings or the housing of gearboxes to measure the vibration responses. In the first step, all the gears are in perfect condition and signals are collected. Then, a damaged gear is installed in the gearbox and signals are collected. The fault symptoms are investigated by comparing the signals from the healthy gearbox with those from the gearbox with a damaged gear. However, these experimental signals are polluted by noise. The fault symptoms may be submerged by the noise and hard to be observed. More importantly, the above comparison between signals can hardly reveal the fault physics of a gearbox.

Feng and Zuo [9] proposed a mathematical model to investigate fault symptoms of a planetary gearbox with tooth pitting. In their model, amplitude modulation and frequency modulation caused by pitting damage are considered. However, their model cannot be used to model pitting growth. In addition, their mathematical model lacks the connection with physical parameters of a gearbox, like gear mesh stiffness and damping [10, 11].

Several researchers investigated dynamic properties of a gearbox with tooth pitting through dynamic simulation. Chaari et al. [12], Cheng et al. [13], and Abouel-seoud et al. [14] modeled a single tooth pit in the rectangular shape (all other teeth are perfect) and investigated the single tooth pit effect on the dynamic properties of a gearbox. Rincon et al. [15] modeled an elliptical pit on a single tooth and evaluated the dynamic force of a pair of gears. Ma et al. [16] studied the effect of tooth spalling on gear mesh stiffness. A single rectangular spalling was modeled and the effects of spalling width, spalling length and spalling location on stiffness were investigated, respectively. Saxena et al. [17] incorporated the gear tooth friction effect in modeling a single gear tooth spalling. Liang et al. [18] evaluated the mesh stiffness of gears with multiple pits on a single tooth using the potential energy method. However, all these studies focus on single tooth

pitting modeling. According to the current studies [3, 19], pitting propagation to neighboring teeth is a common phenomenon. This study overcomes the shortcomings of single tooth pitting modeling. We will model gear tooth pitting propagation to neighboring teeth and analyze its effect on gearbox vibration.

Gear dynamic models may provide useful information for fault diagnosis [20]. Vibration-based time domain, frequency domain, and time-frequency domain analyses provide powerful tools for fault diagnosis of rotating machinery [21, 22]. One traditional technique is based on statistical measurements of vibration signals [23]. Many statistical indicators were proposed for machine fault diagnosis [24–27]. In Liu et al. [25], 34 statistical indicators were summarized and 136 features were generated. In Zhao et al. [26], 63 statistical indicators were summarized and 252 features were produced. The features [25, 26] were used for the classification of gear damage levels of a lab planetary gearbox. In this study, 36 statistical indicators are selected from the literature. Then, 114 statistical features are generated and tested using simulated vibration signals for the pitting growth estimation of a fixed-axis gearbox. The effect of gear mesh damping and environmental noise on the performance of statistical features will be analyzed.

The objective of this study is to simulate vibration signals of gears with tooth pitting covering multiple teeth, investigate pitting effects on vibration properties and provide effective features for pitting growth estimation. The scope of this paper is limited to a fixed-axis gearbox with a single pair of spur gears. A dynamic model is used to investigate the effects of tooth pitting growth on vibration properties of a gearbox. The tooth pitting propagation to the neighboring teeth is modeled. Three pitting levels are modeled: slight pitting, moderate pitting and severe pitting. The vibration signals of a gearbox are simulated for each of the three severity levels. The vibration properties are investigated and fault symptoms are summarized. Statistical features are tested on simulated vibration signals. These features are ranked for pitting growth estimation. The features insensitive to gear mesh damping and environmental noise are recommended.

This paper is organized as follows. In Section 1, an introduction of this study is given including literature review, our research scope and objective. In Section 2, a pitting propagation model and a method to evaluate mesh stiffness of gears with tooth pitting are presented. In Section 3, a dynamic model is utilized to simulate vibration signals of a spur gearbox with tooth pitting, and pitting effects on the vibration signals are analyzed. In Section 4, 114 statistical features are tested for estimation of gear tooth pitting propagation, and gear mesh damping and environmental noise effect on these features are analyzed.

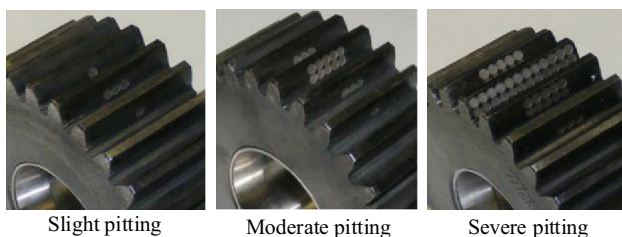


Figure 1 Man-made tooth pitting on gears [8]

In the end, a summary and conclusion of this study is given.

2 Tooth Pitting Propagation Modeling and Mesh Stiffness Evaluation

2.1 Tooth Pitting Propagation Modeling

In this study, we assume the pinion (driving gear) has relatively soft gear tooth surfaces and the gear (driven gear) has surface-hardened teeth. Tooth pitting only propagates in the pinion (the gear is always in perfect condition). Tooth pits are modeled in circular shape [6, 7]. All the circular pits have the diameter of 2 mm and the depth of 1 mm. Three pitting levels are modeled as shown in Figure 2. The detailed information of these three pitting damage levels is given below:

Slight pitting: 9 circular pits on one tooth and 3 circular pits on each of the two neighboring teeth. All the circular pits center on the tooth pitch line. The surface area of the meshing side of a tooth is 194 mm². This way, the middle pitted tooth has a pitting area of 14.6% of the tooth surface area. Each of the two neighboring teeth has a pitting area of 4.87% of the tooth surface area. The purpose of this level of damage is to mimic slight pitting damage that corresponds to the level 2 pitting damage defined in ASM handbook [3].

Moderate pitting: 18 circular pits on one tooth, 9 circular pits on each of the two neighboring teeth, and 3 circular pits on each of the next neighboring teeth on symmetric sides. All the circular pits center on the tooth pitch line. The pitting areas of the 5 teeth are 4.87%, 14.6%, 29.2%, 14.6% and 4.87%, respectively. We call this damage level the moderate pitting damage corresponding to the level 3 pitting damage defined in ASM handbook [3].

Severe pitting: 36 circular pits on one tooth, 18 circular pits on each of the two neighboring teeth, 9 circular pits on each of the next neighboring teeth on symmetric sides and 3 circular pits on each of the teeth after the next neighboring teeth on symmetric sides. For the gear tooth with 36 circular pits, 18 pits center on the tooth pitch line and another 18 pits on the tooth addendum. For other teeth, circular pits all center on the tooth pitch line. The pitting areas of the 7 teeth are 4.87%, 14.6%, 29.2%, 58.4%,

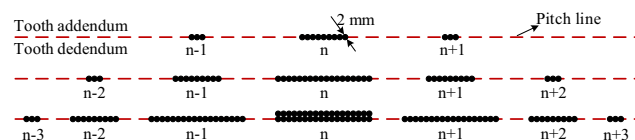


Figure 2 Schematics of pitting damage levels (slight to severe – from top to bottom) on the *n*th tooth of the pinion and its neighboring teeth

29.2%, 14.6% and 4.87%, respectively. We define this level of damage as the severe pitting damage corresponding to the level 4 pitting damage defined in ASM handbook [3].

2.2 Mesh Stiffness Evaluation

Gear mesh stiffness is one of the main internal excitations of gear dynamics. With the growth of gear tooth pitting, gear mesh stiffness shape changes and consequently dynamic properties of gear systems change. Therefore, accurate gear mesh stiffness evaluation is a prerequisite of gear dynamics analysis.

In Ref. [18], the potential energy method [28, 29] was used to evaluate mesh stiffness of gears with multiple pits on a single tooth. The gear tooth was modeled as a non-uniform cantilever beam. The total energy stored in a pair of meshing gears was the sum of Hertzian energy, bending energy, shear energy and axial compressive energy corresponding to Hertzian stiffness, bending stiffness, shear stiffness and axial compressive stiffness, respectively. Their equations are extended here to evaluate the mesh stiffness of gears with tooth pitting distributed over multiple neighboring teeth. The gear system is assumed to be without friction (perfect lubrication), manufacturing error, or transmission error, and the gear body is treated as rigid [18, 28, 29]. The same assumptions will be employed in this paper as this study only focuses on pitting effect on vibration properties.

Figure 3 shows a gear tooth modeled as a non-uniform cantilever beam. The tooth fillet curve is approximated using a straight line for the convenience of equation derivation [29]. Each circular pit is expressed by three variables [18]: (*u*, *r*, *δ*), where *u* represents the distance between the tooth root and the circle center of the pit, *r* is the radius of the pit circle, and *δ* is the pitting depth.

If many circular pits show on a surface, as long as the pits do not overlap with each other and all are within the tooth surface area, the Hertzian contact stiffness *k_h*,

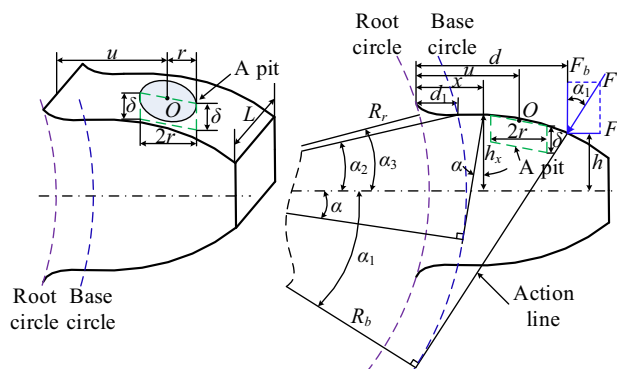


Figure 3 A gear tooth with a circular pit [18]

bending stiffness k_b , shear stiffness k_s and axial compressive stiffness k_a can be expressed as follows [18]:

$$k_h = \frac{\pi E(L - \sum^N \Delta L_{xj})}{4(1 - \nu^2)}, \tag{1}$$

$$\frac{1}{k_b} = \frac{\left[1 - \frac{(Z-2.5)\cos\alpha_1\cos\alpha_3}{Z\cos\alpha_0}\right]^3 - (1 - \cos\alpha_1\cos\alpha_2)^3}{2EL\cos\alpha_1\sin^3\alpha_2} + \int_{-\alpha_1}^{\alpha_2} \frac{3\{1 + \cos\alpha_1[(\alpha_2 - \alpha)\sin\alpha - \cos\alpha]\}^2(\alpha_2 - \alpha)\cos\alpha}{E\left(2L[\sin\alpha + (\alpha_2 - \alpha)\cos\alpha]^3 - 3\sum_1^N \frac{\Delta A_{yj}}{R_b^3}\right)} d\alpha, \tag{2}$$

$$\frac{1}{k_s} = \frac{1.2(1 + \nu)\cos^2\alpha_1\left(\cos\alpha_2 - \frac{Z-2.5}{Z\cos\alpha_0}\cos\alpha_3\right)}{EL\sin\alpha_2} + \int_{-\alpha_1}^{\alpha_2} \frac{1.2(1 + \nu)(\alpha_2 - \alpha)\cos\alpha\cos^2\alpha_1}{E\left(L[\sin\alpha + (\alpha_2 - \alpha)\cos\alpha] - 0.5\sum_1^N \frac{\Delta A_{yj}}{R_b}\right)} d\alpha, \tag{3}$$

$$\frac{1}{k_a} = \frac{\sin^2\alpha_1\left(\cos\alpha_2 - \frac{Z-2.5}{Z\cos\alpha_0}\cos\alpha_3\right)}{2EL\sin\alpha_2} + \int_{-\alpha_1}^{\alpha_2} \frac{(\alpha_2 - \alpha)\cos\alpha\sin^2\alpha_1}{E\left(2L[\sin\alpha + (\alpha_2 - \alpha)\cos\alpha] - \sum_1^N \frac{\Delta A_{yj}}{R_b}\right)} d\alpha, \tag{4}$$

where E , L , ν denote Young’s modulus, tooth width and Poisson’s ratio, respectively; Z is the number of gear teeth; N represents the number of circular pits on a tooth surface; α_0 is the pressure angle; α_1 denotes the angle between action force F and its decomposition component F_b ; α_2 indicates the half tooth angle on the base circle; α_3 describes the approximated half tooth angle on the root circle; ΔL_{xj} , ΔA_{xj} and ΔI_{xj} (caused by the j th circular pit) represent respectively the reduction of tooth contact width, area and area moment of inertia of the tooth section where the distance to the tooth root is x ; ΔL_{xj} , ΔA_{xj} and ΔI_{xj} are expressed as follows [18]:

$$\Delta L_x = \begin{cases} 2\sqrt{r^2 - (u - x)^2}, & x \in [u - r, u + r], \\ 0, & \text{others,} \end{cases} \tag{5}$$

$$\Delta A_x = \begin{cases} \Delta L_x \delta, & x \in [u - r, u + r], \\ 0, & \text{others,} \end{cases} \tag{6}$$

$$\Delta I_x = \begin{cases} \frac{1}{12}\Delta L_x \delta^3 + \frac{A_x \Delta A_x (h_x - \delta/2)^2}{A_x - \Delta A_x}, & x \in [u - r, u + r], \\ 0, & \text{others.} \end{cases} \tag{7}$$

Eqs. (1)–(4) are derived for a single gear tooth (with pitting) which is modeled as a non-uniform cantilever beam. They are all expressed as a function of gear rotation

angle α_1 . Applying these equations iteratively to each gear tooth, the stiffness of each tooth can be obtained. But, the values for ΔL_{xj} , ΔA_{xj} and ΔI_{xj} may be different among teeth due to the variance of number and location of pits.

For a pair of spur gears with contact ratio between 1 and 2, one pair and two pairs of tooth contact takes place alternatively. For a single-tooth-pair meshing duration, the total effective mesh stiffness can be evaluated [18, 28]:

$$k_t = \frac{1}{\frac{1}{k_h} + \frac{1}{k_{b1}} + \frac{1}{k_{s1}} + \frac{1}{k_{a1}} + \frac{1}{k_{b2}} + \frac{1}{k_{s2}} + \frac{1}{k_{a2}}}, \tag{8}$$

where subscripts 1 and 2 represent the driving gear and the driven gear, respectively.

For a double-tooth-pair meshing duration, there are two pairs of gears meshing at the same time. The total effective mesh stiffness can be obtained as [18, 28]:

$$k_t = k_{t1} + k_{t2} = \sum_{i=1}^2 \frac{1}{\frac{1}{k_{h,i}} + \frac{1}{k_{b1,i}} + \frac{1}{k_{s1,i}} + \frac{1}{k_{a1,i}} + \frac{1}{k_{b2,i}} + \frac{1}{k_{s2,i}} + \frac{1}{k_{a2,i}}}, \tag{9}$$

where $i = 1$ for the first pair and $i = 2$ for the second pair of meshing teeth.

Utilizing the above equations, mesh stiffness of a pair of spur gears (gear parameters are given in Table 1) is evaluated for each of the three pitting severity levels as shown in Figure 2. The mesh stiffness results are shown in Figure 4. When angular displacement of the pinion is 0, tooth $n-3$ (see Figure 2) starts to mesh. Gear mesh stiffness reduces when the pitted teeth mesh. Table 2 summarizes the quantifications of stiffness reduction caused by tooth pitting. The averaged mesh stiffness reduction δ_k is used

Table 1 Physical parameters of a spur gearbox [11]

Parameter	Pinion (driving)	Gear (driven)
Number of teeth	19	31
Module (mm)	3.2	3.2
Pressure angle	20°	20°
Mass (kg)	0.700	1.822
Face width (m)	0.0381	0.0381
Young’s modulus (GPa)	206.8	206.8
Poisson’s ratio	0.3	0.3
Base circle radius (mm)	28.3	46.2
Root circle radius (mm)	26.2	45.2
Bearing stiffness (N/m)	$k_1 = k_2 = 5.0 \times 10^8$	
Bearing damping (kg/s)	$c_1 = c_2 = 4 \times 10^5$	
Torsional stiffness of shaft coupling (N/m)	$k_p = k_g = 4.0 \times 10^7$	
Torsional damping of shaft coupling (kg/s)	$c_p = c_g = 3 \times 10^4$	

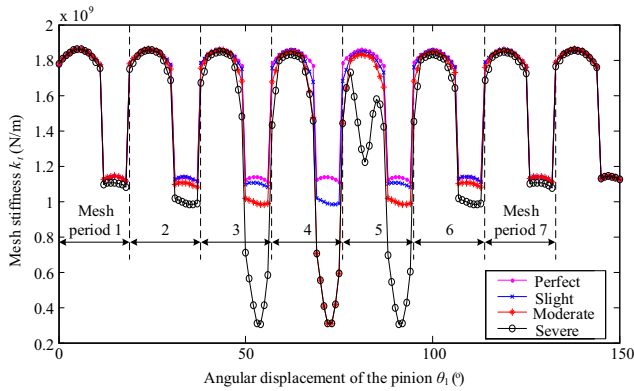


Figure 4 Pitting effect on gear mesh stiffness

Table 2 Averaged mesh stiffness reduction (%) caused by tooth pitting

Mesh period No.	Double-tooth-pair meshing duration			Single-tooth-pair meshing duration		
	Slight	Moderate	Severe	Slight	Moderate	Severe
1	0	0	0.18	0	0	2.84
2	0	0.18	1.04	0	2.83	11.61
3	0.18	1.06	3.27	2.86	11.70	55.78
4	1.04	3.20	5.38	11.61	55.33	55.37
5	1.57	4.26	19.02	2.87	11.73	55.83
6	0.40	1.54	4.17	0	2.87	11.68
7	0	0.41	1.56	0	0	2.86
8	0	0	0.40	0	0	0

to quantify the mesh stiffness reduction. It is defined as follows [18]:

$$\delta_{-k_t} = \left(\left| \frac{\sum_{s=1}^S k_{t1s}}{S} - \frac{\sum_{m=1}^M k_{t2m}}{M} \right| / \frac{\sum_{m=1}^M k_{t2m}}{M} \right) \times 100\%, \quad (10)$$

where k_{t1} and k_{t2} are the mesh stiffness calculated for a damaged gear and a perfect gear, respectively, and S and M represent the mesh stiffness data points collected during the same angular displacement for a damaged gear and a perfect gear, respectively.

Eight mesh periods (see Figure 4) are analyzed in Table 2 because only the mesh stiffness of these eight mesh periods may be affected in our model during one revolution of the pinion. One mesh period is defined as an angular displacement of the pinion experiencing a double-tooth-pair meshing duration and a single-tooth-pair meshing duration. For double-tooth-pair meshing durations, 4, 6 and 8 mesh periods have mesh stiffness reduction caused by slight pitting, moderate pitting and severe pitting, respectively. The maximum averaged mesh stiffness reduction in a double-

tooth-pair meshing duration is 1.57%, 4.26% and 19.02% corresponding to slight pitting, moderate pitting and severe pitting, respectively. While for single-tooth-pair meshing durations, 3, 5 and 7 mesh periods experience mesh stiffness reduction corresponding to slight pitting, moderate pitting and severe pitting, respectively. The maximum averaged mesh stiffness reduction in a single-tooth-pair meshing duration is 11.61%, 55.33% and 55.83% related to slight pitting, moderate pitting and severe pitting, respectively. For each mesh period, the stiffness reduction in the single-tooth-pair meshing duration is larger than that in the double-tooth-pair meshing duration for two reasons: (a) the pitting mostly appear around the pitch line and the pitch line lies on the single-tooth-pair meshing duration, and (b) the perfect gear has a smaller averaged mesh stiffness in the single-tooth-pair meshing duration than the double-tooth-pair meshing duration. In the following section, the pitting effect on the vibration properties of a spur gearbox will be investigated.

3 Dynamic Simulation of a Fixed-axis Gearbox

3.1 Dynamic Modeling

A dynamic model (see Figure 5) reported in Bartelmus [30] is used directly in this study for gear pitting effect analysis. This model had been used in dynamic analysis of gears with tooth crack [23, 31, 32]. It is a mass-spring-

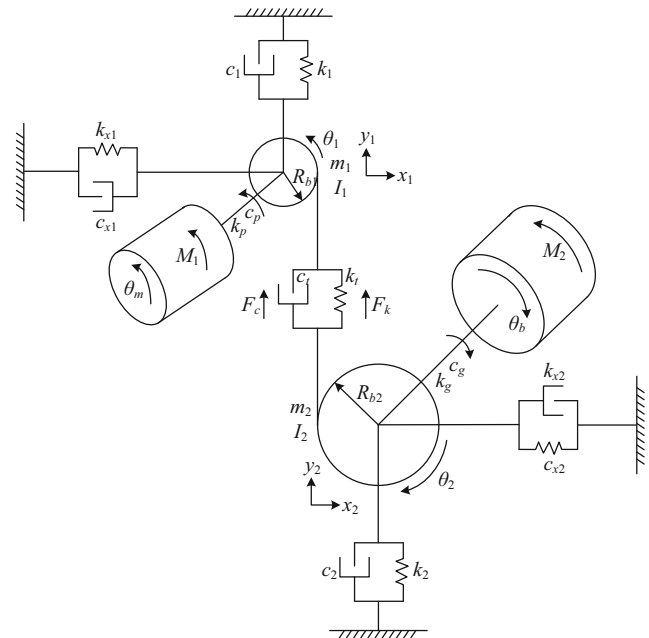


Figure 5 One stage gearbox system [30]

damper (8 degrees of freedom) dynamic model with both torsional and lateral vibrations considered. The system is driven by an electric motor with an input torque M_1 and loaded with torque M_2 . The motor shaft and the shaft that the pinion mounts on are coupled with a flexible coupling. Similarly, the shaft of the load and the shaft that the gear mounts on are coupled with a flexible coupling. In this model, the x -direction vibration is uncoupled with the y -direction vibration [31]. We pay our attention to the y -direction vibration since this direction is along with the direction of gear dynamic force.

To emphasize gear fault symptoms caused by tooth pitting, this model ignored transmission errors, the frictions between gear teeth, and other practical phenomena, such as backlash. In addition, we assume the gearbox casing is rigid so that the vibration propagation along the casing is linear as did in Ref. [31]. Consequently, the vibration response properties of gears in lateral directions are consistent with those on the gearbox casing.

Only consider the motion in the y -direction. The motion equations are given as follows [30]:

$$m_1\ddot{y}_1 + c_1\dot{y}_1 + k_1y_1 = -F_k - F_c, \quad (11)$$

$$m_2\ddot{y}_2 + c_2\dot{y}_2 + k_2y_2 = F_k + F_c, \quad (12)$$

$$I_1\ddot{\theta}_1 = k_p(\theta_m - \theta_1) + c_p(\dot{\theta}_m - \dot{\theta}_1) - R_{b1}(F_k + F_c), \quad (13)$$

$$I_2\ddot{\theta}_2 = R_{b2}(F_k + F_c) - k_g(\theta_2 - \theta_b) - c_g(\dot{\theta}_2 - \dot{\theta}_b), \quad (14)$$

$$I_m\ddot{\theta}_m = M_1 - k_p(\theta_m - \theta_1) - c_p(\dot{\theta}_m - \dot{\theta}_1), \quad (15)$$

$$I_b\ddot{\theta}_b = -M_2 + k_g(\theta_2 - \theta_b) + c_g(\dot{\theta}_2 - \dot{\theta}_b), \quad (16)$$

$$F_k = k_t(R_{b1}\theta_1 - R_{b2}\theta_2 + y_1 - y_2), \quad (17)$$

$$F_c = c_t(R_{b1}\dot{\theta}_1 - R_{b2}\dot{\theta}_2 + \dot{y}_1 - \dot{y}_2). \quad (18)$$

The related notations are listed as follows: c_1 – Vertical damping of the input bearing, c_2 – Vertical damping of the output bearing, c_g – Torsional damping of the output shaft coupling, c_p – Torsional damping of the input shaft coupling, c_t – Gear mesh damping, c_{x1} – x -direction damping of the input bearing, c_{x2} – x -direction damping of the output bearing, f_m – Gear mesh frequency, f_s – Rotation frequency of the pinion, I_1 – Mass moment of inertia of the pinion, I_2 – Mass moment of inertia of the gear, I_b – Mass moment of inertia of the load, I_m – Mass moment of inertia of the driving motor, k_g – Torsional stiffness of the output shaft coupling, k_p – Torsional stiffness of the input shaft coupling, k_t – Gear mesh stiffness, k_1 – y -direction stiffness of the input bearing, k_2 – y -direction stiffness of the output bearing, k_{x1} – x -direction stiffness of the input bearing, k_{x2} – x -direction stiffness of the output bearing, R_{b1} – Base circle radius of the pinion, R_{b2} – Base circle radius of the gear, x_1 – x -direction displacement of the pinion, x_2 – x -direction displacement of the gear, y_1 – y -direction displacement of

the pinion, y_2 – y -direction displacement of the gear, θ_1 – Angular displacement of the pinion, θ_2 – Angular displacement of the gear, θ_b – Angular displacement of the load, θ_m – Angular displacement of the driving motor.

3.2 Numerical Simulation

To investigate pitting effects on vibration properties, vibration signals are simulated for a gearbox of which physical parameters are given in Table 1. Gear mesh damping is considered to be proportional to gear mesh stiffness as did in Amabili and Rivola [33]. The gear mesh damping ratio is selected to be 0.07. Four health conditions are considered: perfect condition and three pitting severity levels as shown in Figure 2. A constant torque of 11.9 N·m is generated by the driving motor and the shaft speed of load is constrained to be 18.4 Hz. Correspondingly, the theoretical rotation speed of the pinion is 30 Hz (f_s) and the gear mesh frequency (f_m) is 570 Hz. The torque and speed values come from Refs. [18, 31]. Numerical results are obtained using MATLAB *ode15 s* solver with sampling frequency of 100000. The time duration of simulated signals covers four revolutions of the pinion.

Figure 6 gives y -direction displacement signals of the pinion for perfect condition, slight pitting condition, moderate pitting condition and severe pitting condition, respectively. The time duration of all signals given in this figure is 0.033 s corresponding to one revolution of the pinion. In one revolution of the pinion, 19 gear meshes go through as the pinion has 19 teeth. We can see 19 big spikes in the perfect condition corresponding to these 19 gear meshes. The amplitude of these spikes are almost the same because all the teeth are in perfect condition. For the slight pitting, the fault symptom is very weak, but careful observation can see one spike (pointed by an arrow) is slightly bigger than others. This spike is mainly generated by the n th tooth (9 pits, pitted area 14.6%) as indicated in Figure 2. For the moderate pitting, one bigger spike is mainly induced by the n th tooth (18 pits, pitted area 29.2%) and two slightly bigger spikes (pointed by arrows) are mainly caused by the $(n-1)$ th tooth (9 pits, pitted area 14.6%) and the $(n+1)$ th tooth (9 pits, pitted area 14.6%), respectively. For the severe pitting, three bigger spikes are mainly caused by the $(n-1)$ th tooth (18 pits, pitted area 29.2%), the n th tooth (36 pits, pitted area 58.4%) and the $(n+1)$ th tooth (18 pits, pitted area 29.2%), respectively. In addition, two slightly bigger spikes (pointed by arrows) are mainly generated by the $(n-2)$ th tooth (9 pits, pitted area 14.6%) and the $(n+2)$ th tooth (9 pits, pitted area 14.6%), respectively. Overall, when the pitted area is below about 15%, the fault symptom is very weak for visual observation, while when the pitted area reaches about 30%, the fault symptom is obvious.

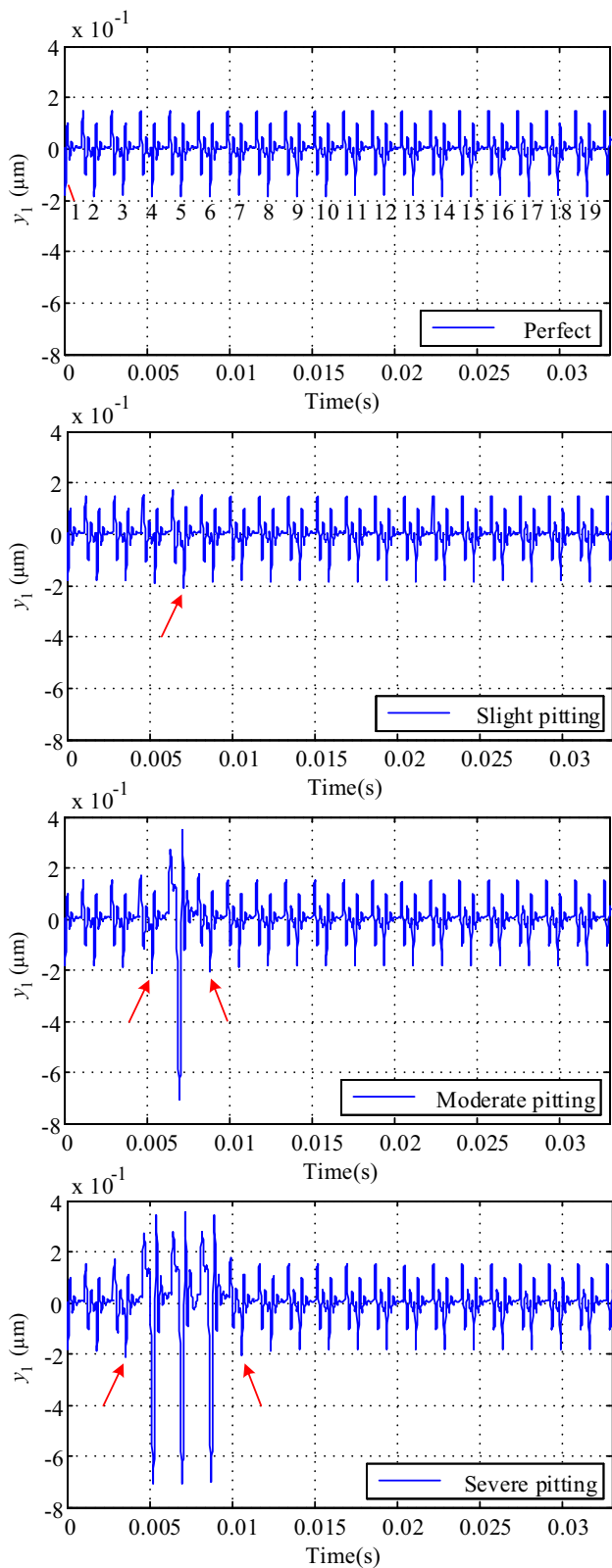


Figure 6 Displacement signals of the pinion for four health conditions of gearbox (the arrows point at weak fault symptoms)

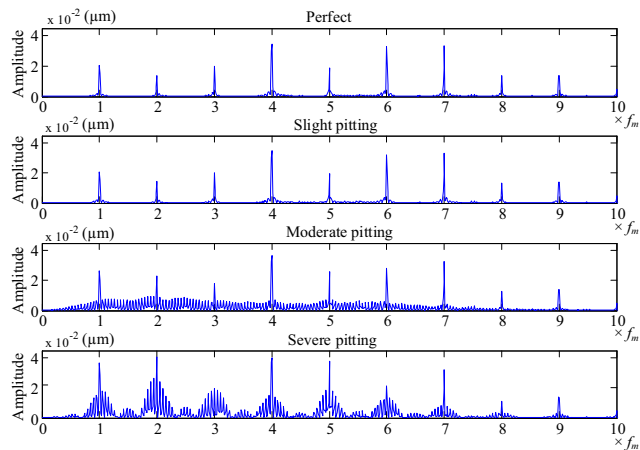


Figure 7 Frequency spectrum of the simulated vibration signals (f_m is gear mesh frequency)

Figure 7 shows frequency spectrum of the simulated vibration signals obtained using the fast Fourier transform. Four health conditions (perfect, slight pitting, moderate pitting and severe pitting) are analyzed. Sizable amplitudes show at gear mesh frequency (f_m) and its harmonics under all the four health conditions. In the perfect and slight pitting conditions, the gear mesh frequency and its harmonics dominate the frequency spectrum (the sideband amplitude is very small). While in the moderate pitting and severe pitting conditions, a large number of sidebands appear around the gear mesh frequency and its harmonics.

Figure 8 presents the zoomed-in frequency spectrum of the simulated vibration signals under the health conditions of moderate pitting and severe pitting, respectively. The frequency interval between sidebands is the characteristic frequency of the pitted pinion (f_s , rotation frequency of the pinion). We can observe that the gear mesh frequency is modulated by the characteristic frequency of the pitted

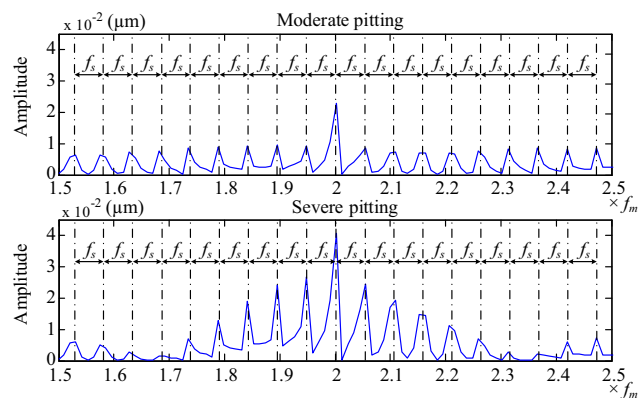


Figure 8 Zoomed-in frequency spectrum of simulated vibration signals (f_m is gear mesh frequency)

Table 3 Definition of thirty-six statistical indicators [25]

Feature	Name	Definition
F_1	Maximum value	The maximum value in $x(n)$, i.e., $\max(x(n))$
F_2	Minimum value	The minimum value in $x(n)$, i.e., $\min(x(n))$
F_3	Mean	$\bar{x} = \frac{1}{N} \sum_{n=1}^N x(n)$
F_4	Peak to peak	$\max(x(n)) - \min(x(n))$
F_5	Harmonic mean	$\frac{N}{\sum_{n=1}^N \frac{1}{x(n)}}$
F_6	Trimmed mean	Mean excluding outliers
F_7	Variance	$\frac{1}{N} \sum_{n=1}^N (x(n) - \bar{x})^2$
F_8	Standard deviation	$\sqrt{\frac{1}{N} \sum_{n=1}^N (x(n) - \bar{x})^2}$
F_9	Mean absolute deviation	$\frac{1}{N} \sum_{n=1}^N x(n) - \bar{x} $
F_{10}	Median absolute deviation	$\frac{1}{N} \sum_{n=1}^N x(n) - x_{\text{median}} $
F_{11}	Interquartile range	The 1st quartile subtracted from the 3rd quartile
F_{12}	Peak2RMS	$\frac{\max(x(n))}{\sqrt{\frac{1}{N} \sum_{n=1}^N x(n)^2}}$
F_{13}	Skewness	$\frac{\frac{1}{N} \sum_{n=1}^N (x(n) - \bar{x})^3}{\left(\sqrt{\frac{1}{N} \sum_{n=1}^N (x(n) - \bar{x})^2}\right)^3}$
F_{14}	Kurtosis	$\frac{\frac{1}{N} \sum_{n=1}^N (x(n) - \bar{x})^4}{\left(\frac{1}{N} \sum_{n=1}^N (x(n) - \bar{x})^2\right)^2}$
F_{15}	Shape factor	$\frac{\sqrt{\frac{1}{N} \sum_{n=1}^N x(n)^2}}{\frac{1}{N} \sum_{n=1}^N x(n) }$
F_{16}	Crest factor	$\frac{\max(x(n))}{\sqrt{\frac{1}{N} \sum_{n=1}^N x(n)^2}}$
F_{17}	Clearance factor	$\frac{\max(x(n))}{\frac{1}{N} \sum_{n=1}^N x(n)^2}$
F_{18}	Impulse factor	$\frac{\max(x(n))}{\frac{1}{N} \sum_{n=1}^N x(n) }$

Table 3 continued

Feature	Name	Definition
F_{19}	Third order central moment	$\frac{1}{N} \sum_{n=1}^N (x(n) - \bar{x})^3$
F_{20}	Fourth order central moment	$\frac{1}{N} \sum_{n=1}^N (x(n) - \bar{x})^4$
F_{21}	Root mean square	$\sqrt{\frac{1}{N} \sum_{n=1}^N x(n)^2}$
F_{22}	Energy operator	$\frac{\frac{1}{N} \sum_{n=1}^N (\Delta x(n) - \Delta \bar{x})^4}{\left(\frac{1}{N} \sum_{n=1}^N (\Delta x(n) - \Delta \bar{x})^2\right)^2}$
F_{23}	Mean frequency	$\frac{1}{K} \sum_{k=1}^K X(k)$
F_{24}	Frequency center	$\frac{\sum_{k=1}^K (f(k) \times X(k))}{\sum_{k=1}^K X(k)}$
F_{25}	Root mean square frequency	$\sqrt{\frac{\sum_{k=1}^K (f(k)^2 \times X(k))}{\sum_{k=1}^K X(k)}}$
F_{26}	Standard deviation frequency	$\sqrt{\frac{\sum_{k=1}^K ((f(k) - F_{28})^2 \times X(k))}{\sum_{k=1}^K X(k)}}$
F_{27}	NA4	$\frac{\frac{1}{N} \sum_{n=1}^N (r(n) - \bar{r})^4}{\left(\frac{1}{M} \sum_{m=1}^M \left(\frac{1}{N} \sum_{n=1}^N (r_m(n) - \bar{r}_m)^2\right)\right)^2}$
F_{28}	NA4*	$\frac{\frac{1}{N} \sum_{n=1}^N (r(n) - \bar{r})^4}{\left(\frac{1}{M} \sum_{m=1}^M \frac{1}{N} \sum_{n=1}^N (r_m(n) - \bar{r}_m)^2\right)^2}$
F_{29}	FM4	$\frac{\frac{1}{N} \sum_{n=1}^N (d(n) - \bar{d})^4}{\left(\frac{1}{N} \sum_{n=1}^N (d(n) - \bar{d})^2\right)^2}$
F_{30}	FM4*	$\frac{\frac{1}{N} \sum_{n=1}^N (d(n) - \bar{d})^4}{\left(\frac{1}{M} \sum_{m=1}^M \left(\frac{1}{N} \sum_{n=1}^N (d_m(n) - \bar{d}_m)^2\right)\right)^2}$
F_{31}	M6A	$\frac{\frac{1}{N} \sum_{n=1}^N (d(n) - \bar{d})^6}{\left(\frac{1}{N} \sum_{n=1}^N (d(n) - \bar{d})^2\right)^3}$

Table 3 continued

Feature	Name	Definition
F_{32}	M6A*	$\frac{\frac{1}{N} \sum_{n=1}^N (d(n) - \bar{d})^6}{\left(\frac{1}{M'} \sum_{m=1}^{M'} \left(\frac{1}{N} \sum_{n=1}^N (d_m(n) - \bar{d}_m)^2 \right) \right)^3}$
F_{33}	M8A	$\frac{\frac{1}{N} \sum_{n=1}^N (d(n) - \bar{d})^8}{\left(\frac{1}{N} \sum_{n=1}^N (d(n) - \bar{d})^2 \right)^4}$
F_{34}	M8A*	$\frac{\frac{1}{N} \sum_{n=1}^N (d(n) - \bar{d})^8}{\left(\frac{1}{M'} \sum_{m=1}^{M'} \left(\frac{1}{N} \sum_{n=1}^N (d_m(n) - \bar{d}_m)^2 \right) \right)^4}$
F_{35}	NB4	$\frac{\frac{1}{N} \sum_{n=1}^N (e(n) - \bar{e})^4}{\left(\frac{1}{M'} \sum_{m=1}^{M'} \left(\frac{1}{N} \sum_{n=1}^N (e_m(n) - \bar{e}_m)^2 \right) \right)^2}$
F_{36}	NB4*	$\frac{\frac{1}{N} \sum_{n=1}^N (e(n) - \bar{e})^4}{\left(\frac{1}{M'} \sum_{m=1}^{M'} \left(\frac{1}{N} \sum_{n=1}^N (e_m(n) - \bar{e}_m)^2 \right) \right)^2}$

* means a variant of the original indicator

pinion (f_s). The degree of frequency modulation increases with the degree of damage of the pitting. In addition, sidebands near gear mesh frequency and its harmonics increase obviously with the growth of tooth pitting severity.

4 Estimation of Pitting Growth Using Statistical Features

In Section 3, we analyzed vibration properties of a spur gearbox for four health conditions (perfect condition and three pitting severity levels). In this section, we test the effectiveness of thirty-six statistical indicators (see Table 3) for estimation of pitting growth. Four types of signals are used for the tests: raw signals (RAW), residual signals (RES), difference signals (DIFF), and first-order sideband signals (FSB). RAW denotes the simulated vibration signals in the Section 3 with the mean subtracted. RES is obtained by removing gear mesh frequencies and their harmonics from the RAW. DIFF is generated by removing the first-order sidebands from the RES. FSB represents the signals containing only the first-order sidebands. Twenty-six statistical indicators (F_1 to F_{26}) are

applied to each of the four type signals. Therefore, 104 (26×4) features can be generated. The statistical indicators F_{27} and F_{28} are only applied to RES since they were originally proposed for RES [34]. Similarly, the statistical indicators F_{29} to F_{34} are only applied to DIFF since they are specially designed for DIFF [27]. The statistical indicators F_{35} and F_{36} are only applied to FSB [27]. In total, we generate 114 ($104 + 10$) features for estimation of pitting growth.

This paragraph explains the symbols used in the expressions of the 36 statistical indicators as listed in Table 3. We use $x(n)$, $r(n)$, $d(n)$, and $b(n)$ to represent RAW, RES, DIFF, and FSB, respectively. The symbol $X(k)$, $k = 1, 2, \dots, K$, represents the k th measure of the frequency spectrum of a signal. The symbol $f(k)$ denotes frequency amplitude of the k th spectrum component. The bar notation represents mean, e.g., \bar{x} is the mean of $x(n)$. The symbols $r_m(n)$, $d_m(n)$ and $b_m(n)$ denote the m th time record of $r(n)$, $d(n)$ and $b(n)$, respectively. The symbol $e(n)$ represents the envelope of the current time record, which is expressed as $e(n) = |b(n) + j \times H(b(n))|$, where $H(b(n))$ is the Hilbert transform of $b(n)$. $e_m(n)$ represents the envelope of the m th time record of $b(n)$. M describes the total number of time records up to present. M' represents the total number of time records for a healthy gearbox. In this study, M and M' equal to 1 for simplicity. A signal $x(n)$ is looped around to calculate $\Delta x(n) = x(n)^2 - x(n-1)x(n+1)$.

Pearson correlation coefficient (PCC) is utilized to quantify the effectiveness of these 114 features. It is a metric to estimate the linear relationship between a single statistical feature and its corresponding label. Its range is $[-1, 1]$. The value closer to one indicates a better statistical feature for pitting growth estimation. The expression of PCC [35] is given below:

Table 4 Features with a PCC value greater than 0.97

Ranking	Feature	PCC	Ranking	Feature	PCC
1	RAW- F_{11}	0.9843	12	RES- F_{10}	0.9718
2	FSB- F_6	0.9743	13	FSB- F_8	0.9714
3	RES- F_9	0.9742	14	FSB- F_{21}	0.9714
4	RES- F_{11}	0.9739	15	FSB- F_4	0.9713
5	RAW- F_8	0.9737	16	FSB- F_9	0.9710
6	RAW- F_1	0.9737	17	FSB- F_1	0.9708
7	DIFF- F_{11}	0.9737	18	RES- F_7	0.9707
8	RAW- F_9	0.9736	19	DIFF- F_9	0.9704
9	DIFF- F_{10}	0.9735	20	FSB- F_{10}	0.9704
10	FSB- F_{26}	0.9727	21	FSB- F_{25}	0.9701
11	FSB- F_{23}	0.9721			

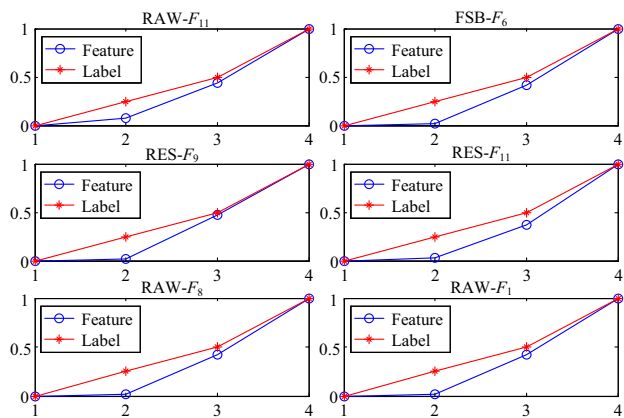


Figure 9 Best six features (the numbers 1, 2, 3 and 4 in the x -axis represent the health conditions of perfect, slight pitting, moderate pitting and severe pitting, respectively; the y -axis is the normalized feature values)

$$\rho = \frac{\sum_{i=1}^N (x_i - \bar{x})(y_i - \bar{y})}{\sqrt{\sum_{i=1}^N (x_i - \bar{x})^2} \sqrt{\sum_{i=1}^N (y_i - \bar{y})^2}}, \tag{19}$$

where x_i and y_i represent a feature value and a label value, respectively, for the i th health condition of a gearbox; \bar{x} and \bar{y} are the means of \mathbf{x} ($\mathbf{x} = [x_1, x_2, \dots, x_N]^T$) and \mathbf{y} ($\mathbf{y} = [y_1, y_2, \dots, y_N]^T$), respectively; and N is the number of health conditions. In this study, N is equal to four, and $\mathbf{y} = [0, 0.146, 0.292, 0.584]^T$. The elements in \mathbf{y} correspond to the largest tooth pitted area of the pinion in the health conditions of perfect, slight pitting, moderate pitting and severe pitting, respectively.

Test results give that only one feature (RAW- F_8) achieves a PCC value of greater than 0.98 while 21 features can get a PCC value of greater than 0.97. These 21 features and their PCC values are given in Table 4. Figure 9 presents performances of the best six features: RAW- F_{11} , FSB- F_6 , RES- F_9 , RES- F_{11} , RAW- F_8 , and RAW- F_1 . Their PCC values are 0.9843, 0.9743, 0.9742, 0.9739, 0.9737, and 0.9737, respectively. RAW- F_{11} means the statistical indicator F_{11} (see Table 3) is tested on RAW. Other features can be interpreted in the same way. The feature values are linearly normalized to values between 0 and 1 in Figure 9 using the following equation:

$$V_{normalized} = \frac{(V_{current} - V_{perfect})}{(V_{severe} - V_{perfect})}, \tag{20}$$

where $V_{current}$ denotes the feature value in current health condition of a gearbox, $V_{perfect}$ is the feature value in perfect condition, and V_{severe} represents the feature value in severe pitting condition.

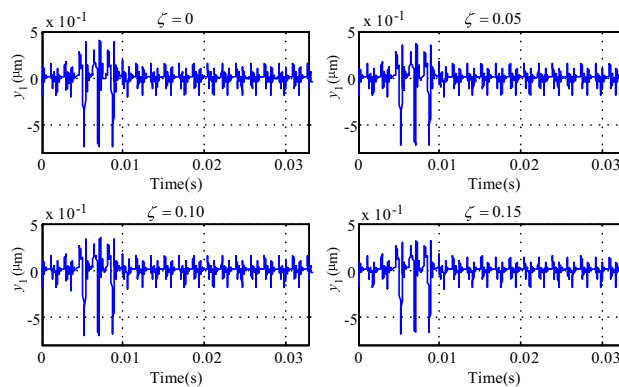


Figure 10 Gear mesh damping effect on gear vibration under severe pitting condition

From Figure 9, we can see that the best six features share the similar increase trend with the tooth pitting propagation. The feature values change very slightly from perfect to slight pitting even for the best feature RAW- F_{11} (see Figure 9), which indicates the features are not sensitive to slight pitting. This is because fault symptoms are very weak under the slight pitting health condition (see Figure 6). From slight pitting to moderate pitting and from moderate pitting to severe pitting, a large change of feature values can be observed from the top six features. Therefore, it is much easier to detect moderate pitting and severe pitting than slight pitting.

4.1 Gear Mesh Damping Effect on the Effectiveness of Statistical Features

In many studies, gear mesh damping is ignored or considered to be constant [36–38]. Li and Kahraman [39] demonstrated that it was not proper to use a constant gear mesh damping. Amabili and Rivola [33] modeled the gear mesh damping proportional to gear mesh stiffness and investigated damping effect on the steady state response of a pair of spur gears. In most situations, gear mesh damping ratio ranges from 0.01 to 0.1 [33, 39, 40]. This study does not intend to propose a new model for gear mesh damping. Our focus is to test gear mesh damping effect on the effectiveness of statistical indicators. The gear mesh damping model reported in Amabili and Rivola [33] is used directly in this study.

$$c_t = 2\zeta \sqrt{\frac{m_1 m_2}{m_1 + m_2}} k_t, \tag{21}$$

where m_1 and m_2 represents the mass of the pinion and the gear, respectively, k_t and c_t denotes the gear mesh stiffness and damping, respectively, and ζ is gear mesh damping ratio.

Table 5 Top 10 features for each damping condition

Feature ranking	$\zeta = 0$		$\zeta = 0.05$	
	Feature	PCC	Feature	PCC
1	RAW- F_{10}	0.9896	RAW- F_{11}	0.9885
2	RAW- F_{11}	0.9885	FSB- F_6	0.9747
3	FSB- F_{26}	0.9768	RES- F_9	0.9745
4	FSB- F_6	0.9747	RES- F_{11}	0.9744
5	RES- F_9	0.9746	FSB- F_{26}	0.9742
6	RAW- F_{21}	0.9736	DIFF- F_{10}	0.9739
7	RAW- F_8	0.9736	RAW- F_9	0.9739
8	DIFF- F_{11}	0.9735	RAW- F_8	0.9739
9	RAW- F_9	0.9735	RAW- F_{21}	0.9739
10	DIFF- F_{10}	0.9732	DIFF- F_{11}	0.9738
Feature ranking	$\zeta = 0.1$		$\zeta = 0.15$	
	Feature	PCC	Feature	PCC
1	RAW- F_{11}	0.9843	RAW- F_5	0.9903
2	FSB- F_6	0.9746	RAW- F_{11}	0.9859
3	RES- F_{11}	0.9744	FSB- F_6	0.9746
4	RAW- F_8	0.9742	DIFF- F_{11}	0.9744
5	RAW- F_{21}	0.9742	DIFF- F_{10}	0.9742
6	RES- F_9	0.9741	RES- F_9	0.9740
7	RAW- F_9	0.9738	RAW- F_9	0.9739
8	DIFF- F_{11}	0.9734	RAW- F_{21}	0.9739
9	DIFF- F_{10}	0.9733	RAW- F_8	0.9739
10	FSB- F_{23}	0.9720	RES- F_{11}	0.9735

Table 6 Top 10 features for each noise level

Feature ranking	No noise		10 db	
	Feature	PCC	Feature	PCC
1	RAW- F_{11}	0.9843	DIFF- F_5	0.9806
2	FSB- F_6	0.9743	DIFF- F_{10}	0.9791
3	RES- F_9	0.9742	DIFF- F_{11}	0.9790
4	RES- F_{11}	0.9739	RES- F_{11}	0.9769
5	RAW- F_8	0.9737	RES- F_{10}	0.9769
6	RAW- F_1	0.9737	RAW- F_8	0.9756
7	DIFF- F_{11}	0.9737	RAW- F_{21}	0.9756
8	RAW- F_9	0.9736	RES- F_9	0.9746
9	DIFF- F_{10}	0.9735	RAW- F_9	0.9741
10	FSB- F_{26}	0.9727	RAW- F_{10}	0.9737
Feature ranking	0 db		-10 db	
	Feature	PCC	Feature	PCC
1	FSB- F_{22}	0.9953	RAW- F_1	0.9887
2	FSB- F_1	0.9813	FSB- F_{23}	0.9755
3	RES- F_{22}	0.9803	DIFF- F_{11}	0.9739
4	FSB- F_{21}	0.9783	DIFF- F_{10}	0.9736
5	FSB- F_8	0.9783	RAW- F_8	0.9727
6	FSB- F_4	0.9778	RAW- F_{21}	0.9727
7	FSB- F_9	0.9774	RAW- F_9	0.9720
8	FSB- F_{23}	0.9747	DIFF- F_{23}	0.9717
9	FSB- F_{35}	0.9743	RAW- F_{23}	0.9717
10	RES- F_4	0.9741	RES- F_{23}	0.9716

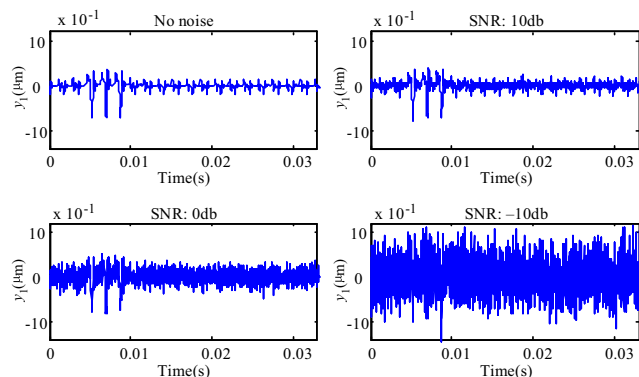


Figure 11 Environmental noise effect on gear vibration under severe pitting condition

Using the dynamic model in Section 3, four damping conditions are tested: no damping, damping ratio of 0.05, damping ratio of 0.10 and damping ratio of 0.15. Figure 10 gives an example to illustrate gear mesh damping effect on gear vibration under severe pitting condition. From visual observation, there is no big difference. To quantify the difference, the root mean square is calculated for the

signals to be 1.13 μm , 1.09 μm , 1.06 μm and 1.04 μm corresponding to no damping, damping ratio of 0.05, damping ratio of 0.10 and damping ratio of 0.15, respectively. Signal amplitude decreases slightly with the increase of damping ratio.

Table 5 gives top 10 features for each damping condition. Eight features perform very well. They belong to the top 10 in all damping conditions. These eight features are RAW- F_{11} , FSB- F_6 , RES- F_9 , RAW- F_{21} , RAW- F_8 , DIFF- F_{11} , RAW- F_9 and DIFF- F_{10} . Damping has negligible effect on the performance of these eight features.

4.2 Environmental Noise Effect on the Effectiveness of Statistical Features

For the simulated signals, there is no environmental noise involved. In real applications, environmental noise always exists. White Gaussian noise is added to the simulated signals to mimic the environmental noise [41, 42]. Four noise levels are tested: no noise, signal-to-noise ratio (SNR) of 10 db, SNR of 0 db and SNR of -10 db.

Table 7 Top 10 stable features

Features	PCC			
	No noise	10 db	0 db	-10 db
RAW- F_{11}	0.9842	0.9735	0.9697	0.9699
RES- F_9	0.9742	0.9746	0.9708	0.9711
RAW- F_8	0.9737	0.9756	0.9727	0.9727
RAW- F_{21}	0.9737	0.9756	0.9727	0.9727
RAW- F_9	0.9736	0.9740	0.9719	0.9719
DIFF- F_{10}	0.9735	0.9791	0.9705	0.9736
RAW- F_7	0.9691	0.9704	0.9681	0.9697
RAW- F_{20}	0.9673	0.9674	0.9597	0.9548
RES- F_{28}	0.9625	0.9626	0.9505	0.9526
RES- F_{20}	0.9625	0.9626	0.9505	0.9526

Figure 11 shows the environmental noise effect on gear vibration under severe pitting condition. With the increase of noise level, the fault symptom becomes weaker and weaker. Under SNR of -10 db, the gear fault symptoms are not visible any more on the time domain waveform.

Table 6 gives top 10 features for each noise level. Noise has a larger effect on the performance of features than gear mesh damping. None of the features is the shared top 10 among the four noise levels. Some features perform well under low noise level condition but perform badly under strong noise condition. These features cannot be used if background noise is strong. Some features have a large fluctuation on performance with the variation of noise level. These features are not suggested to use since their performance is not stable. Good features should be insensitive to noise variation.

Table 7 summarizes the top 10 features with relatively stable performance. The PCC value of these 10 stable features is insensitive to noise level variation. To avoid the influence of both gear mesh damping and environmental noise, 6 features are suggested to use. They are RAW- F_{11} , RES- F_9 , RAW- F_8 , RAW- F_{21} , RAW- F_9 , DIFF- F_{10} . These 6 features belong to both the top 8 features selected in Section 4.1 considering gear mesh damping effect and the top 10 stable features selected in Section 4.2 considering environmental noise effect. They are insensitive to neither gear mesh damping nor environmental noise.

Time Synchronous Averaging can remove interference frequencies induced by environmental noise and other irrelevant machine components [43]. But, there is no environmental noise in the simulated signals. Other machine components of the simulated spur gear pair are represented by constant damping and constant stiffness parameters and as a result, there are no irrelevant frequency components caused by other machine components. As shown in Figures 7 and 8, only the gear mesh frequency

and the pinion pitting fault induced sideband frequency components are present. When a more complex gearbox system is simulated, TSA may be needed. However, in real applications, especially for the slight pitting damage scenario, TSA and subsequent feature extraction may not be adequate for effective fault detection and diagnosis. Advanced signal processing techniques, such as empirical mode decomposition and wavelet analysis, may be used together with TSA for more effective fault detection and diagnosis.

5 Conclusions

This study investigates effects of pitting growth on vibration properties of a spur gearbox and tests the effectiveness of 114 features to estimate the pitting growth. The pitting propagation to neighboring teeth is modeled using circular pits. The potential energy method is applied to evaluate gear mesh stiffness of a pair of spur gears for each of the four health conditions: the perfect condition, the slight pitting, the moderate pitting and the severe pitting. An eight degrees of freedom torsional and lateral dynamic model is used to simulate gearbox vibration signals. Pitting growth effects on vibration properties of a spur gearbox are analyzed. These properties can give insights into developing new signal processing methods for gear tooth pitting diagnosis. At the end, 114 features are tested to estimate the pitting growth. The features are ranked based on the Absolute Pearson Correlation Coefficient. The statistical features insensitive to gear mesh damping and environmental noise is recommended. However, further investigation of these selected features based on experimental signals is still needed before potential field applications. Our next step is to design and conduct experiments on a lab gearbox with introduced gear tooth pitting and refine the features proposed in this paper.

Open Access This article is distributed under the terms of the Creative Commons Attribution 4.0 International License (<http://creativecommons.org/licenses/by/4.0/>), which permits unrestricted use, distribution, and reproduction in any medium, provided you give appropriate credit to the original author(s) and the source, provide a link to the Creative Commons license, and indicate if changes were made.

References

1. X H Liang, M J Zuo, W H Chen. *Dynamics based vibration signal modeling for tooth fault diagnosis of planetary gearboxes*, Chapter 7 in: M. Demetgul, M. Ünal (Eds.), *Fault Diagnosis and Detection*, In Tech, 2017: 175–192.
2. M R Hoseini, M J Zuo. *Literature review for creating and quantifying faults in planetary gearboxes*. Reliability Research Lab, Mechanical Department, University of Alberta, May 2009.

3. ASM Committee. *Friction, lubrication, and wear technology*. American Society for Microbiology (ASM) International, 1992.
4. L Gelman, R Zimroz, J Birkel, et al. Adaptive vibration condition monitoring technology for local tooth damage in gearboxes. *Insight - Non-Destructive Testing & Condition Monitoring*, 2005, 47: 461–464.
5. S K Lee, J S Shim, B O Cho. Damage detection of a gear with initial pitting using the zoomed phase map of continuous wavelet transform. *Key Engineering Materials*, 2006, 306–308: 223–228.
6. F Combet, L Gelman. Optimal filtering of gear signals for early damage detection based on the spectral kurtosis. *Mechanical Systems and Signal Processing*, 2009, 23: 652–668.
7. H Öztürk, M Sabuncu, I Yesilyurt. Early detection of pitting damage in gears using mean frequency of scalogram. *Journal of Vibration and Control*, 2008, 14: 469–484.
8. M R Hoseini, Y G Lei, D V Tuan, et al. *Experiment design of four types of experiments: pitting experiments, run-tofailure experiments, various load and speed experiments, and crack experiments*. Reliability Research Lab, Mechanical Department, University of Alberta, January 2011.
9. Z P Feng, M J Zuo. Vibration signal models for fault diagnosis of planetary gearboxes. *Journal of Sound and Vibration*, 2012, 331: 4919–4939.
10. X H Liang, M J Zuo, T H Patel. Evaluating the time-varying mesh stiffness of a planetary gear set using the potential energy method. *Proceedings of the Institution of Mechanical Engineers, Part C: Journal of Mechanical Engineering Science*, 2014, 228(3): 535–547.
11. X H Liang, M J Zuo, M R Hoseini. Vibration signal modeling of a planetary gear set for tooth crack detection. *Engineering Failure Analysis*, 2015, 48: 185–200.
12. F Chaari, W Baccar, M S Abbes, et al. Effect of spalling or tooth breakage on gearmesh stiffness and dynamic response of a one-stage spur gear transmission. *European Journal of Mechanics - A/Solids*, 2008, 27: 691–705.
13. Z Cheng, N Q Hu, F S Gu, et al. Pitting damage levels estimation for planetary gear sets based on model simulation and grey relational analysis. *Transactions of the Canadian Society for Mechanical Engineering*, 2011, 35: 403–417.
14. S A Abouel-seoud, E S Dyab, M S Elmorsy. Influence of tooth pitting and cracking on gear meshing stiffness and dynamic response of wind turbine gearbox. *International Journal of Science and Advanced Technology*, 2012, 2: 151–165.
15. A F Rincon, F Viadero, M Iglesias, et al. Effect of cracks and pitting defects on gear meshing. *Proceedings of the Institution of Mechanical Engineers, Part C: Journal of Mechanical Engineering Science*, 2012, 226: 2805–2815.
16. H Ma, Z W Li, M J Feng, et al. Time-varying mesh stiffness calculation of spur gears with spalling defect. *Engineering Failure Analysis*, 2016, 66: 166–176.
17. A Saxena, A Parey, M Chouksey. Time varying mesh stiffness calculation of spur gear pair considering sliding friction and spalling defects. *Engineering Failure Analysis*, 2016, 70: 200–211.
18. X H Liang, H S Zhang, L B Liu, et al. The influence of tooth pitting on the mesh stiffness of a pair of external spur gears. *Mechanism and Machine Theory*, 2016, 106: 1–15.
19. C K Tan, P Irving, D Mba. A comparative experimental study on the diagnostic and prognostic capabilities of acoustics emission, vibration and spectrometric oil analysis for spur gears. *Mechanical Systems and Signal Processing*, 2007, 21: 208–233.
20. X H Liang, M J Zuo, Z P Feng. Dynamic modeling of gearbox faults: A review. *Mechanical Systems and Signal Processing*, 2018, 98: 852–876.
21. T H Patel, A K Darpe. Experimental investigations on vibration response of misaligned rotors. *Mechanical Systems and Signal Processing*, 2009, 23: 2236–2252.
22. T H Patel, A K Darpe. Coupled bending-torsional vibration analysis of rotor with rub and crack. *Journal of Sound and Vibration*, 2009, 326: 740–752.
23. S Y Wu, M J Zuo, A Parey. Simulation of spur gear dynamics and estimation of fault growth. *Journal of Sound and Vibration*, 2008, 317: 608–624.
24. X M Zhao, M J Zuo, Z L Liu. Diagnosis of pitting damage levels of planet gears based on ordinal ranking. *IEEE Conference on Prognostics and Health Management (PHM)*, Denver, USA, June 20–23, 2011: 1–8.
25. Z L Liu, J Qu, M J Zuo, et al. Fault level diagnosis for planetary gearboxes using hybrid kernel feature selection and kernel fisher discriminant analysis. *The International Journal of Advanced Manufacturing Technology*, 2012, 67: 1217–1230.
26. X M Zhao, M J Zuo, Z L Liu, et al. Diagnosis of artificially created surface damage levels of planet gear teeth using ordinal ranking. *Measurement*, 2013, 46: 132–144.
27. P D Samuel, D J Pines. A review of vibration-based techniques for helicopter transmission diagnostics. *Journal of Sound and Vibration*, 2005, 282: 475–508.
28. D CH Yang, J Y Lin. Hertzian damping, tooth friction and bending elasticity in gear impact dynamics. *Journal of Mechanical Design*, 1987, 109: 189–196.
29. X H Liang, M J Zuo, M Pandey. Analytically evaluating the influence of crack on the mesh stiffness of a planetary gear set. *Mechanism and Machine Theory*, 2014, 76: 20–38.
30. W Bartelmus. Mathematical modelling and computer simulations as an aid to gearbox diagnostics. *Mechanical Systems and Signal Processing*, 2001, 15: 855–871.
31. X H Tian, M J Zuo, K R Fyfe. Analysis of the vibration response of a gearbox with gear tooth faults. *ASME International Mechanical Engineering Congress and Exposition*, Anaheim, California, USA, November 13–20, 2004: 785–793.
32. Z G Tian, M J Zuo, S Y Wu. Crack propagation assessment for spur gears using model-based analysis and simulation. *Journal of Intelligent Manufacturing*, 2012, 23: 239–253.
33. M Amabili, A Rivola. Dynamic analysis of spur gear pairs: steady-state response and stability of the SDOF model with time-varying meshing damping. *Mechanical Systems and Signal Processing*, 1997, 11: 375–390.
34. P Večeř, M Kreidl, R Šmíd. Condition indicators for gearbox condition monitoring systems. *Acta Polytech*, 2005, 45(6): 35–43.
35. Z L Liu, M J Zuo, H Xu. Fault diagnosis for planetary gearboxes using multi-criterion fusion feature selection framework. *Proceedings of the Institution of Mechanical Engineers, Part C: Journal of Mechanical Engineering Science*, 2013, 227: 2064–2076.
36. J Lin, R G Parker. Analytical characterization of the unique properties of planetary gear free vibration. *Journal of Vibration and Acoustics*, 1999, 121: 316–321.
37. A Saxena, A Parey, M Chouksey. Dynamic analysis of multi-mesh geared rotor system using modal analysis. *Prognostics & System Health Management Conference*, Chengdu, China, Oct. 16–22, 2016: 1–5.
38. X H Liang, M J Zuo, L B Liu. A windowing and mapping strategy for gear tooth fault detection of a planetary gearbox. *Mechanical Systems and Signal Processing*, 2016, 80: 445–459.
39. S Li, A Kahraman. A spur gear mesh interface damping model based on elasto-hydrodynamic contact behaviour. *International Journal of Powertrains*, 2011, 1: 4–21.
40. A S Kumar, T S Sankar, M O M Osman. On dynamic tooth load and stability of a spur-gear system using the state-space approach.

Journal of Mechanism, Transmissions, and Automation in Design, 1985, 107: 54–60.

41. Z P Feng, M J Zuo. Fault diagnosis of planetary gearboxes via torsional vibration signal analysis. *Mechanical Systems and Signal Processing*, 2013, 36: 401–421.
42. Y F Li, X H Liang, M J Zuo. Diagonal slice spectrum assisted optimal scale morphological filter for rolling element bearing fault diagnosis. *Mechanical Systems and Signal Processing*, 2017, 85: 146–161.
43. E Bechhoefer, M Kingsley. A review of time synchronous average algorithms. *Annual Conference of the Prognostics and Health Management Society*, San Diego, CA, September, 2009: 24–33.

Xi-Hui Liang, is currently a postdoctoral research fellow at *Reliability Research Lab, University of Alberta, Canada*. His research interests include dynamic modeling of mechanical systems, condition monitoring, fault diagnostics and prognostics, asset management, reliability analysis, maintenance, solid mechanics, finite element analysis, and intelligent manufacturing. E-mail: xihui2@ualberta.ca

Zhi-Liang Liu, is an associate professor at *University of Electronic Science and Technology of China, China*. His research interests

mainly include machinery fault diagnosis and prognosis by using signal processing and data mining techniques. He published more than 30 papers including 10 + journal papers. He currently held 7 research grants from National Natural Science Foundation of China, Open Grants of National Key Laboratory, China Postdoctoral Science Foundation, etc. E-mail: Zhiliang_Liu@uestc.edu.cn

Jun Pan, is a professor at *ZhejiangSci-Tech University, China*. He received the master degree from *Zhejiang University, China*, in 2002 and the Ph.D. degree from *ZhejiangSci-Tech University, China*, in 2011. His research interests include modeling and statistical analysis of accelerated life testing/degradation testing, design of testing plans, and estimation of system reliability. E-mail: panjun@zstu.edu.cn

Ming Jian Zuo, is a professor at the *University of Alberta, Canada*. His research interests include system and network reliability modeling and analysis, reliability based optimal design, multi-state system performance evaluation, condition monitoring and fault diagnosis, maintenance optimization, and manufacturing system modeling and planning. E-mail: ming.zuo@ualberta.ca